A Lattice Boltzmann method for turbulent emulsions

A Lattice Boltzmann method for turbulent emulsions

Luca Biferale[1,2], Prasad Perlekar[2], Mauro Sbragaglia[1], Sudhir Srivastava[2] and Federico Toschi[2,3]

[1] Department of Physics, University of Tor Vergata, Italy.
[2] Department of Physics and Department of Mathematics and Computer Science, Eindhoven University of Technology, Eindhoven 5600MB, The Netherlands.
[3] CNR-IAC, Via dei Taurini 19, 00185, Rome, Italy.

E-mail: biferale@roma2.infn.it, p.perlekar@tue.nl, sbragaglia@roma2.infn.it, s.srivastava@tue.nl, f.toschi@tue.nl

Abstract. The breakup of droplets in a turbulent flow is key to many natural and industrial applications. Here we present and validate a computationally efficient numerical method that allows to study turbulent emulsion for very long times. The numerical method is based on a multi-component Lattice Boltzmann method based on the Shan-Chen model and supplemented with a large scale force to stir turbulence. A special treatment to limit mobility between different fluid components is introduced and validated. We demonstrate the potential of our approach in sustaining a turbulent emulsion over extremely long integration times (necessary to collect firm turbulence statistics) and we present first results on the probability distribution function of droplets' accelerations.

1. Introduction

The breakup of fluid droplets in turbulent flows is relevant to many natural and industrial application because turbulence is an ubiquitous state of fluid motion. Control of turbulent emulsions is relevant to application in chemical engineering, pharmaceutical, food, and oil industries.

In recent years there has been a large effort in understanding the properties of particles and small droplets with different physical properties transported by turbulent flows field. These studies involved both experimental and numerical investigations and mostly focused on the effects of particles density and size (Toschi & Bodenschatz, 2009). Most of the studies were conducted in the context of the so called one-way coupling, where the particles are transported by the turbulence velocity field but do not react back on it or interact with each other. This assumption is a good approximation for particles that are not too big (Calzavarini *et al.*, 2009) and allows for the collection of extraordinary high statistics.

In order to investigate the behavior of droplets in turbulent flows in regimes where deformation and breakup are important, one needs a method capable of fully resolving droplets evolution. In this study we use the Lattice Boltzmann Method (LBM) as an efficient computational tool to collect stationary statistical information.

In the past the Lattice Boltzmann Method (LBM) has been successfully applied to the study of droplets breakup in laminar shear flows (Xi & Duncan, 1998), as well to the study of turbulent flows of single-phase single-component fluids (Benzi & Succi, 1990; Kareem *et al.*, 2009; Yu *et al.*,

2005). The LBM was able to successfully reproduce Taylor's prediction for the small droplet deformation regime and also to capture their breakup (Xi & Duncan, 1998). Some work has also been done to apply the LBM to turbulent emulsions but studies here were limited only to the earlier stages of the emulsion evolution (Benzi & Succi, 1990; Derksen & Akker, 2007; Qian *et al.*, 2006). The breakup of bubbles in homogeneous and isotropic turbulence reported the formation of stretched liquid bridges connecting the satellite droplets just before the breakup occurs (Qian *et al.*, 2006).

In this paper we show that a multicomponent LBM can be effectively used to study the long time *statistically steady* dispersion of droplets in a homogeneous and isotropic turbulent velocity flow. For the sake of simplicity we focus only on the case of droplets with the same density and viscosity of the turbulent fluid environment. While the numerical method does not have this restriction, this allows considering only one additional physical feature, namely the presence of droplet surface tensions. We are interested in investigating the regime of droplets larger than the dissipative scale of turbulence that get largely deformed and eventually broken by the turbulent pressure fluctuations.

The classical phenomenological picture for droplets breakup in homogeneous and isotropic turbulence velocity fields follows the argument proposed by Hinze in 1955 (Hinze, 1955). Whenever the energy associated to the surface tension is larger than the kinetic energy of fluid fluctuations *at the scale* of the droplet, then the droplet is stable else the droplet breaks. This argument can also be rephrased in terms of a scale dependent Weber number:

$$We(d) = \frac{\rho^m \langle \delta u^2(d) \rangle d}{\sigma}, \tag{1}$$

where ρ^m is the density of the fluid medium around the droplet, σ is the surface tension, d is the diameter of the droplet, $\delta u(d)$ is the velocity difference across the diameter of the droplet, and $\langle\rangle$ indicates statistical averaging of the velocity fluctuations over the droplet diameter. Here we consider the viscosity ratio $\lambda = \mu^d/\mu^m$, and the density ratio $\kappa = \rho^d/\rho^m$ to be unity (superscript d denotes droplet, m denotes the medium).

The manuscript is organized as follows. In section 2 we detail the multiphase LBM and the turbulent forcing that we use. In section 3 we validate the method for droplets deformation in laminar shear flows. In section 4 we improve our method to reduce the mobility between the two components. In section 5 we discuss results from turbulent simulations and finally conclusions are drawn.

2. The numerical method

The multicomponent algorithm that we use is based on a standard Shan-Chen Lattice Boltzmann Method (Shan & Chen, 1993, 1994; Shan & Doolen, 1995). This is a standard method and here we provide only the key details. In order to stir turbulence we supplement the method with a large scale forcing in order to keep the system in a stationary turbulent state.

The lattice Boltzmann equations for the Shan-Chen multicomponent D3Q19 model are:

$$f_i^\alpha(\boldsymbol{x} + \boldsymbol{e}_i, t+1) = f_i^\alpha(\boldsymbol{x}) - \frac{1}{\tau_\alpha}[f_i^\alpha(\boldsymbol{x}, t) - f_i^{eq,\alpha}(\rho, \boldsymbol{u})] \tag{2}$$

$$f_i^{eq,\alpha} = \rho^\alpha w_i \left[1 + \frac{\boldsymbol{e}_i \cdot \boldsymbol{u}}{c_s^2} + \frac{\boldsymbol{u}\boldsymbol{u} : (\boldsymbol{e}_i\boldsymbol{e}_i - c_s^2 \boldsymbol{I})}{2c_s^4}\right] \tag{3}$$

$$\rho^\alpha = \sum_i f_i^\alpha; \ \boldsymbol{u}^\alpha(\boldsymbol{x}, t) = \sum_i \boldsymbol{c}_i f_i^\alpha(\boldsymbol{x}, t). \tag{4}$$

Here $f_i^\alpha(\boldsymbol{x}, t)$ is the lattice Boltzmann distribution function at position $\boldsymbol{x}$ and time t describing the component $\alpha = \{1, 2\}$.The fluid densities and the velocities of the individual components are

ρ^α and $\boldsymbol{u}^\alpha$. w_i, $\boldsymbol{e}_i$ are the lattice Boltzmann weights and the corresponding lattice speeds with $i = \{0, \ldots, 18\}$ (Succi, 2001; Wolf-Galdrow, 2000). The total fluid density is $\rho = \sum_\alpha \rho^\alpha$, and the total hydrodynamic velocity is $\boldsymbol{u} = \sum_\alpha u^\alpha \rho^\alpha / \rho$. The effective kinematic viscosity is related to the relaxation time of the different components $\nu = \sum_\alpha c_s^2(\tau^\alpha c^\alpha - 0.5)$ (Shan & Doolen, 1995), $c^\alpha = \rho^\alpha/\rho$ is the concentration, and $c_s = 1/\sqrt{3}$ is the speed of sound on the lattice.

The non-ideal nature of the fluid is introduced by adding an extra force to the lattice Boltzmann equilibrium velocity field as (Shan & Chen, 1994):

$$\boldsymbol{u}^{\alpha,eq} = \boldsymbol{u}' + \frac{\tau^\alpha \boldsymbol{F}^\alpha}{\rho^\alpha} \quad \text{where} \quad \boldsymbol{u}' = \frac{\sum_\alpha \rho^\alpha \boldsymbol{u}^\alpha / \tau^\alpha}{\sum_\alpha \rho^\alpha / \tau^\alpha}. \tag{5}$$

In the present paper we only study the case of a binary mixture. For the non-ideal interaction we use a Shan-Chen force that has the form (Shan & Chen, 1994):

$$F^\alpha = -G\rho^\alpha(\boldsymbol{x}) \sum_{i,\alpha \neq \alpha'} \rho^{\alpha'}(\boldsymbol{x} + \boldsymbol{e}_i) \tag{6}$$

where $\{\alpha, \alpha'\} = \{1, 2\}$ indicate the components and the coupling parameter G determines the strength of the interaction and controls the surface tension and the diffusivity (Benzi *et al.*, 2009). Under appropriate conditions this force allows the formation of interface between the different fluid components.

In order to stir turbulence we apply a real space forcing at each position and at each time step modulated by means of a sum of sine waves with small wavenumbers. In order to produce a homogeneous and isotropic turbulence, the phases of the sine waves are evolved in time by means of a stochastic process. The forcing has the following expression:

$$F_x^\alpha(x, y, z, t) = A\rho^\alpha \sum_{k_x, k_y; k \leq \sqrt{2}} \left[\sin(k_y y + \phi_k^2(t)) + \sin(k_z z + \phi_k^3(t))\right] \tag{7}$$

$$F_y^\alpha(x, y, z, t) = A\rho^\alpha \sum_{k_x, k_z; k \leq \sqrt{2}} \left[\sin(k_x x + \phi_k^1(t)) + \sin(k_z z + \phi_k^3(t))\right] \tag{8}$$

$$F_z^\alpha(x, y, z, t) = A\rho^\alpha \sum_{k_x, k_y; k \leq \sqrt{2}} \left[\sin(k_x x + \phi_k^1(t)) + \sin(k_y y + \phi_k^2(t))\right] \tag{9}$$

where A is an overall forcing amplitude, k_x, k_y, and k_z are the wave-vector components and are limited to $k^2 = k_x^2 + k_y^2 + k_z^2 \leq 2$. The phases ϕ_k^i are evolved in time according to independent Ornstein-Uhlenbeck processes with the same relaxation time $T = u_m/N$, where N is the size of the domain along any of the directions and $u_m \equiv 0.1$ is taken as a representative large scale velocity.

Henceforth, we will denote the physical quantities in droplet phase by superscript d and those of the medium by superscript m. In the following discussions we have chosen $\tau^d = \tau^m = \tau$ which implies $\nu^d = \nu^m = \nu$, i.e. the viscosities of the two phases are the same. Also the total density $\rho^d + \rho^m$ is the same over the entire domain except for the small variations at the droplet interface.

3. Validation

We start by validating the code for the case of a single droplet in a laminar shear flow. Here we compare our measurements against analytical results from Taylor (Taylor, 1932, 1934) and

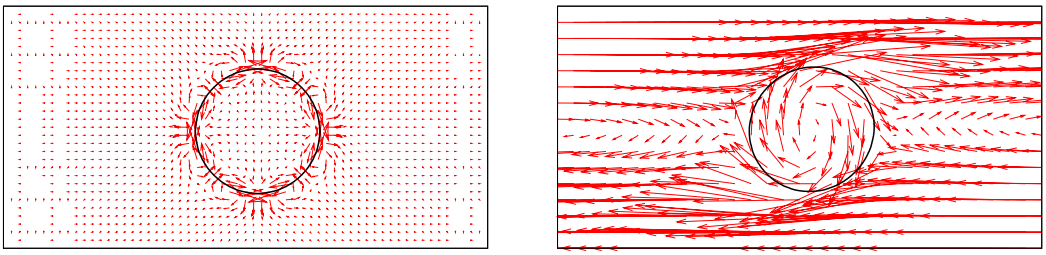

Figure 1. The $2d$ slice cutting a $3d$ droplet through its mid-plane. The black curve indicates the position of the droplet interface separating the two components. (left) Droplet in absence of any flow, notice the spurious currents present at the droplet interface. The magnitude of the maximum velocity in the plane is 1.5×10^{-3}. (right) Deformed droplet in presence of shear for our run `R2` (see Table 1). The velocity has its maximum magnitude at the walls and is equal to 0.006. In both the panel arrows have been magnified by a factor of 8×10^3 to make them visible. The parameters of the simulation are the same as described in Table 1.

we discuss the effects due to the finite interface width as well as related to the mobility between the two components.

We start by considering the case of a droplet in a fluid at rest. The Shan-Chen method (Benzi *et al.*, 2009; Shan & Chen, 1993, 1994; Shan & Doolen, 1995) that we use is a diffused interface numerical method and as such it produces some finite mobility between the two fluid components. Similar to other diffused interface models, the static droplet is surrounded by a complex pattern of unphysical "spurious" velocity between the two components (Sbragaglia *et al.*, 2007). The actual magnitude of the spurious velocity depends on several details, including e.g. the degree of isotropy of the discretization of the gradient in the expression of the Shan-Chen force (Sbragaglia *et al.*, 2007). In Figure 1 we report a two dimensional cut of the velocity field passing through the center of a three dimensional static droplet. Spurious currents are visible in the left panel (Fig. 1) but becomes negligible in a sheared droplet (see right panel of Fig. 1).

In this section we present the benchmark results for the droplet deformation in a shear flow. Our simulation domain consists of a three dimensional box of size N_x, N_y and N_z, with a droplet placed at the center of the box and the other parameters of our simulations as given in Table 1. The shear flow is $\boldsymbol{u} = (2Uy/N_y, 0, 0)$ where U is magnitude of the velocity of the top wall, with a corresponding strain rate $\dot{\gamma} = 2U/N_y$. Depending on the magnitude of the shear and the surface tension of the droplet, the droplet will either deform or break. The relevant non-dimensional parameter here is the capillary number $Ca \equiv \mu\dot{\gamma}R/\sigma$, where $\dot{\gamma}$ is the strain rate, the radius of the undeformed droplet R, and the surface tension σ. For small values of Ca, we observe that the droplet deformation D agrees with the prediction made by Taylor $D = 35/32 \cdot Ca$ (Taylor, 1932, 1934) for small deformations. Deviations are observed for large Ca (Xi & Duncan, 1998), see Figure 2.

The droplet deformation is measured by constructing the symmetric matrix (Xi & Duncan, 1998)

$$A_{ij} = \frac{\int H(\rho^d - \rho_T) x_i x_j dxdydz}{\int H(\rho^d - \rho_T) dxdydz}, \text{and, } H(\rho^d - \rho_T) = \begin{cases} 0 & \text{if } \rho^d < \rho_T \\ 1 & \text{if } \rho^d > \rho_T \end{cases}.$$

where, $\rho_T = (\rho^{d,max} + \rho^{d,min})/2$ is a threshold density. The origin of the coordinate system is at the center of the droplet and $x_i, i = 1, 2, 3$ are the three cartesian coordinate directions. By

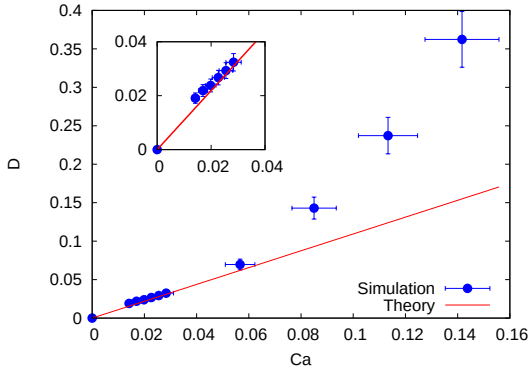

Figure 2. Plot of the capillary number, Ca, versus the droplet deformation, D (see text for details). For small values of Capillary number the droplet deformation follows the Taylor prediction $D = 35/32 \cdot Ca$ (red line). Data in the plots refer to runs `R1` $-$ `R10` (simulation parameters are reported in Table 1). An errorbar of around 10% is reported on our data and is attributed to the finite size of the interface.

diagonalizing the matrix A_{ij}, we calculate the eigenvalues ($\lambda_i, i = 1, 2, 3$, arranged in decreasing order of magnitude) of the matrix . The eigenvalues λ_i are proportional to the three axis of the ellipsoid. We denote the major axis by L and the minor axis by B. The droplet deformation parameter D is then defined as:

$$D \equiv \frac{L - B}{L + B}. \tag{10}$$

We define as mass of the droplet $M \equiv \int_{\rho > \rho_T} \rho^d d\boldsymbol{x}$. The plot in Figure 3 shows the droplet mass for different values of shear S. In these experiments, we allow the droplet to relax for a time T_S, after which we switch on the shear. For smaller values of the shear (e.g. $S = 1.6 \times 10^{-4}$, see run `R1` in Table 1) the droplet mass remains at its thermalized value while on increasing the shear the mass inside the droplets decreases until a new steady state is reached. The most dramatic change occurs for the largest value of the shear attained in our simulations, $S = 3.3 \times 10^{-3}$, where the droplet loses nearly 18% of its original mass after the initialization of shear. We notice that the mass leakage, at least for our closed system, is reversible. This can be seen from the right panel of Figure 3: the mass in the droplet decreases after a shear flow is turned on, and gets back to the no-shear value once the shear is switched off.

4. Control of mass leakage and validation

From Figure 3 it is clear that the mass leakage happens during the transient period when the droplet relaxes towards the new equilibrium after the application of a shear. This mass-leakage is proportional to the mobility which roughly varies as $c_s^2(\tau - 0.5)$ in the Shan-Chen model. One simple and effective way to fix the droplet mass leakage is to reinflate them, while at the same time removing the same amount of fluid from the ambient. As we expect the mass leakage to be proportional to the droplets surface, we apply the re-inflation procedure only at the droplets interface. Here we provide details of the algorithm. In Lattice-Boltzmann the mass can be easily added to the system by locally modifying the populations as $f_i^\alpha = f_i^\alpha + w_i \rho_s^\alpha$, where ρ_s is the density that needs to be added to the component α. The mass cure algorithm is applied after the streaming and collision steps of the LBM using the procedure given below.

(i) We first focus on the distribution function f^d. The regions where the density ρ^d is higher

	N_x	N_y	N_z	U	R_0	σ	Ca	D
R1	128	60	60	0.005	15	0.01	0.014	0.0191
R2	128	60	60	0.006	15	0.01	0.017	0.0219
R3	128	60	60	0.007	15	0.01	0.019	0.0238
R4	128	60	60	0.008	15	0.01	0.022	0.0267
R5	128	60	60	0.009	15	0.01	0.025	0.0293
R6	128	60	60	0.01	15	0.01	0.028	0.0324
R7	128	60	60	0.02	15	0.01	0.055	0.0697
R8	128	60	60	0.04	15	0.01	0.083	0.1430
R9	128	60	60	0.06	15	0.01	0.11	0.2372
R10	128	60	60	0.08	15	0.01	0.138	0.3623

Table 1. Parameters for the different runs with a single droplet in a shear flow. N_x, N_y, and N_z denote the size of the domain along the x, y, and z directions (in lattice sites), U is the absolute value of the velocity at the wall, R_0 is the initial droplet radius, $\nu = c_s^2(\tau - 0.5) = 1/6$ is the viscosity, τ the Lattice Boltzmann relaxation time which we kept the same for the two components, $\sigma = 2\Delta p R_0$ is the surface tension, $\Delta p = p_{in} - p_{out}$ is the pressure jump across the droplet interface, $Ca = 2UR\nu\rho/(N_z\sigma)$ is the capillary number, D is the droplet deformation parameter. In all the runs we kept $\tau = 1$ and $G = -4.5$ fixed.

than the threshold $\rho_T = (\rho^{d,max} + \rho^{d,min})/2$ are considered as droplet interior (indicated as "in"), the rest is considered as droplet exterior (indicated as "out").

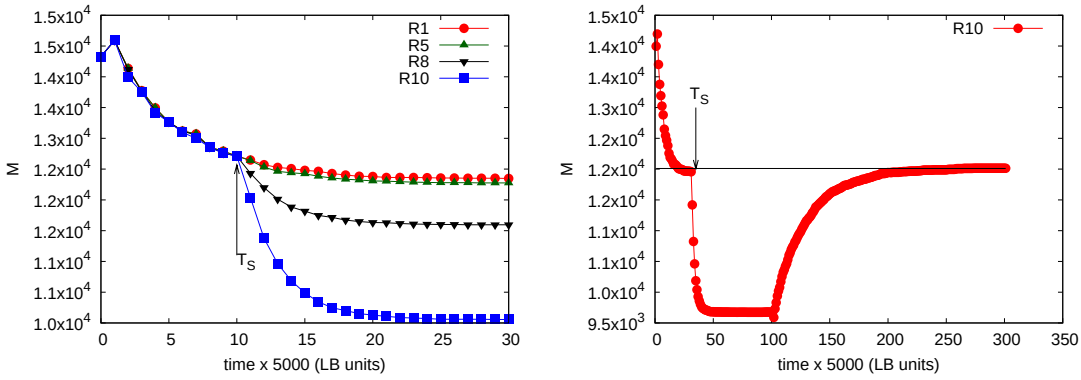

Figure 3. Left panel: droplet mass M versus time for different values of shear $S = 1.6 \times 10^{-4}$ (for run R1), $S = 3.0 \times 10^{-4}$ (for run R5), $S = 1.3 \times 10^{-3}$ (for run R8), and $S = 3.3 \times 10^{-3}$ (for run R10). Parameters of the different runs are reported in Table 1. The vertical arrow indicates the time T_S after which the shear was applied. Note that for the largest shear the droplet looses nearly 18% of its mass. Right panel: droplet mass after a shear-noshear cycle. The droplet is allowed to relax for around 15000 time steps, after which the mass is about 12000. The shear is applied around time step 20000 and a dramatic mass leakage is observed until a new steady state is attained. Switching off the shear around time step 500000 one observe that the droplet reverts back to its old equilibrium. It should be noted that the time it takes for the droplet to get back to the older equilibrium is much longer than the time for mass leakage.

(ii) The cure for the droplet is defined at the droplets interface only, as:

$$\begin{aligned} f_i^d &= f_i^d + A_1|\nabla\rho^d|w_i(\rho^d - \rho_T), \text{ (inside the droplet)} \\ f_i^d &= f_i^d + A_2|\nabla\rho^d|w_i(\rho^d - \rho_T) \text{ (outside the droplet)} \end{aligned}$$

and where the gradient term $|\nabla\rho^d| = \sqrt{(\partial_x\rho^d)^2 + (\partial_y\rho^d)^2 + (\partial_z\rho^d)^2}$ weights more the points within the interface.

(iii) The unknowns A_1 and A_2 are determined by enforcing that after the cure, the mass of the droplet should be $m^{d,in} = \int_{\rho^d>\rho_T} \rho^d d\boldsymbol{x}$ ($m^{d,out} = \int_{\rho^d<\rho_T} \rho^d d\boldsymbol{x}$) inside (outside) the droplet. This choice guarantees that the total mass of the component $m^d = m^{d,in} + m^{d,out}$ remains the same before and after the cure. The coefficients A_1 and A_2 are therefore:

$$A_1 = \frac{m^{d,in}(0) - m^{d,in}(t)}{|\nabla\rho^d|[m^{d,in}(t) - m_T^{in}(t)]},\ A_2 = \frac{m^{d,out}(0) - m^{d,out}(t)}{|\nabla\rho^d|[m^{d,out}(t) - m_T^{out}(t)]}.$$

where, $m_T^{in} = \rho_T \int_{\rho^d>\rho_T} d\boldsymbol{x}$ and $m_T^{out} = \rho_T \int_{\rho_d<\rho_T} d\boldsymbol{x}$.

(iv) Finally we cure the distribution function f^m in the symmetric way:

$$\begin{aligned} f_i^m &= f_i^m - A_1|\nabla\rho^d|w_i(\rho^d - \rho_T), \text{ (inside the droplet)} \\ f_i^m &= f_i^m - A_2|\nabla\rho^d|w_i(\rho^d - \rho_T) \text{ (outside the droplet)} \end{aligned}$$

with the same A_1 and A_2 as for f^d. In this way the total mass $\rho^d + \rho^m$ is conserved. The above procedure adds the lost mass to each droplet weighted by the droplet surface area and and it does not effect the physical processes like Ostwald ripening where there is a mass transfer between two droplets because it is the sum of the mass inside all the droplets which is always conserved (no global leakage).

5. Results for droplets in turbulent flows

Here we discuss the case of droplets in turbulent simulations, whose parameters are given in Table 2. The plot in Figure 4(left panel) shows the time evolution of the total kinetic energy $E = 1/2 \int \boldsymbol{u}^2 d\boldsymbol{x}$ and of the enstrophy $\Omega = \int (\boldsymbol{\nabla u})^2 d\boldsymbol{x}$ from run `N128B`. As it can be seen a clear time lag between the peaks of the energy and those of the dissipation demonstrates the presence of an energy cascade and hence of a turbulent flux in the simulation. Figure 4 (right panel) shows the time evolution of the total mass inside droplets from run `N128A` with and without the curing procedure. We observe that because of the multiple breakups and strong deformations in presence of turbulence the droplet, if not cured, can leak mass rather strongly into the ambient phase.

The calculation of the acceleration of the droplet requires the tracking of the center of mass of the droplet along its trajectory, to avoid complications because of multiple breakup and coagulation events we concentrate on the run `N128A`. For this run we produced long, single droplet, trajectories. Here droplet trajectories are extracted at the post-processing stage. To have reasonable droplet tracks we record every $0.05t_{eddy}$ the density and the velocity fields. From the density field, using a threshold ρ_T, we find the regions on the domain occupied by the droplet. We then reconstruct the droplet surface using the GTS surface reconstruction software (`http://gts.sourceforge.net/`) that reconstructs surface and also provides the information about the volume, surface area, and the center of mass of the droplet. A snapshot of the droplet trajectory is shown in Figure 5(a). From the droplet trajectory we can obtain the acceleration by calculating the second derivative of the position along the droplet trajectory. This procedure turns out to be rather noisy due to the errors in the center of mass position of the droplet during

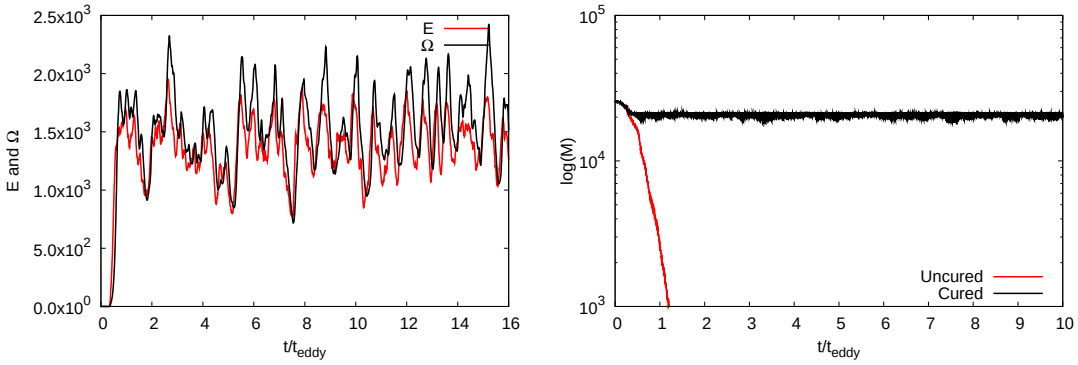

Figure 4. (Left) The time behaviour of the energy and enstrophy integrated over the full simulation domain. The simulation was started with the fluid at rest. After one eddy turnover time $t_{\rm eddy}$ the flow is turbulent as it can be seen from the delay between peaks in the total energy E and enstrophy Ω, demonstrating the presence of an energy cascade. Data refers to run `N128B`. (Right) Plot of the total mass inside the droplet component M for our turbulence run `N128A` versus time for cured versus uncured. We start the cure around $t_{eddy} = 1$. The cure is applied every 0.016 times the large scale eddy turnover time. The inset (left to right) shows the initial and later time snapshot of the droplet configuration. At the initial time the droplet is spherical but at later time, under the effect of turbulence, the droplet deforms and extends.

	N	τ	G	Re_λ	ν	σ	$\phi(in\%)$
`N128A`	128	0.515	0.3	15	5×10^{-3}	0.0016	0.07
`N128B`	128	0.515	0.3	15	5×10^{-3}	0.0016	0.67

Table 2. Parameter for our simulations for a droplet in a homogeneous, isotropic, turbulent flow. N is the size of the tri-periodic domain, $Re_\lambda \equiv u_{rms}\lambda/\nu_m$ is the Taylor's microscale Reynolds number, $\lambda = \sqrt{E/\Omega}$ is the Taylor's microscale, $E = \int \boldsymbol{u}^2 d\boldsymbol{x}$ is the energy, $\Omega = \int |\nabla \boldsymbol{u}|^2$ is the enstrophy, ϕ is the percentage volume fraction of the droplet phase, σ is the surface tension.

the surface reconstruction. To get a better signal we calculate the variance of acceleration after application of a low pass filter. The plot of the variance of acceleration as a function of filter cutoff frequency is shown in Figure 5(b). The frequency where the variance changes the slope is the critical frequency f_c, above which the signal is strongly affected by the noise. We take the acceleration signal filtered with f_c to do the analysis of acceleration pdf (Voth *et al.*, 2002, 1998). We show in Figure 5(a) the filtered and unfiltered acceleration along the droplet trajectory. In Figure 5(right) we plot the droplet acceleration for all droplet trajectories. The comparison of the acceleration with the acceleration evaluated in a single component flow (no droplet) shows that: (a) the level of intermittency of droplet acceleration is lower; and (b) the acceleration of the fluid evaluated over a volume equal to the size of the droplet is similar to the droplet acceleration Figure 5(right).

6. Conclusions

We presented and validated a numerically efficient method for the study of droplets deformation and breakup in turbulent flows. The method is suitable to the study of turbulent emulsion from very small to large volume loading. We demonstrated that by means of a simple numerical aid one can effectively and inexpensively control the diffusivity between the two fluid components allowing for extremely long turbulent simulations. We detailed the algorithm for droplet

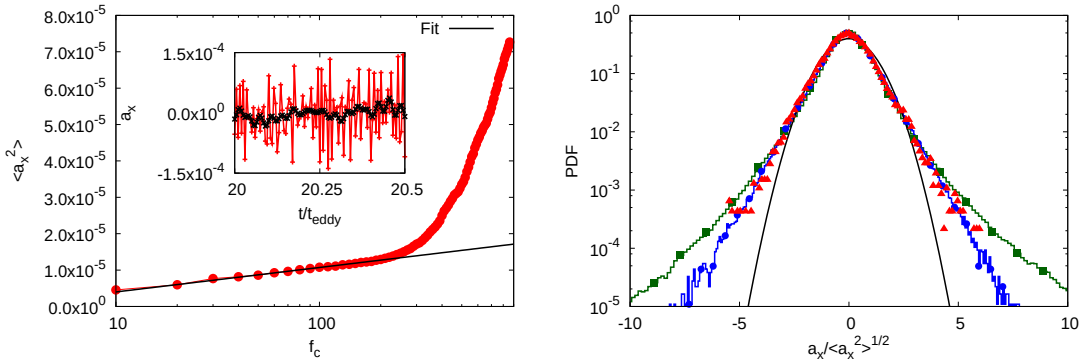

Figure 5. Left panel: Plot showing the root-mean-squared acceleration values as obtained from trajectories low-pass filtered with different cutoff frequencies f_c. At increasing the cutoff frequency more and more high-frequency noise remains in the tracks producing a sharp increase of the a_{rms}. This analysis allow for the choice of the optima filter frequency. (Inset) The time evolution of the droplet acceleration obtained from an unfiltered and from a low-pass filtered droplet trajectory. Right panel: Probability distribution function, pdf, of the droplet acceleration (red triangle), as compared to the pdf of the acceleration for a single component fluid (green line with squares) and the pdf of the acceleration for the single component fluid averaged over a volume of the same size of the droplet (blue line with dots). A reference Gaussian distribution with the same variance is also plotted as reference (black line).

tracking and for the reconstruction of droplets trajectory and acceleration. We measured the probability distribution function and found that this is less intermittent than the one of the advecting velocity field but not distinguishable (within our statistical accuracy) from the one of a rigid droplet of the same finite size. We consider this method promising for the study of droplets emulsions in more complicated regimes, for example in the case of different density or viscosity contrast between the two components. Experimental investigation of deformable droplets tracking would be extremely helpful in exploring how the deformability affects the dynamics of droplets as compared to the one of rigid particles.

Acknowledgements
We thank S. Sundaresan, J. Derksen and H. Xu for discussions. We acknowledge the COST Action MP0806 for support. LB, PP, and FT acknowledge the Kavli Institute of Theoretical Physics for hospitality. This research was supported in part by the National Science Foundation under Grant No. NSF PHY05-51164. We acknowledge computational support from CASPUR (Roma, Italy), from CINECA (Bologna, Italy), and from JSC (Julich, Germany).

References

Benzi, R., Sbragaglia, M., Succi, S., Bernaschi, M. & Chibbaro, S. 2009 Mescoscopic lattice boltzmann modeling of soft-glassy systems: Theory and simulations. *J. Chem. Phys.* **131**, 104903.

Benzi, R. & Succi, S. 1990 Two-dimensional turbulence with the lattice boltzmann equation. *J. Phys. A: Math. Gen.* **23**, L1.

Calzavarini, E., Volk, R., Bourgoin, M., Lèvêque, E., PINTON, J.-F. & TOSCHI, F. 2009 Acceleration statistics of finite-sized particles in turbulent flow: the role of faxén forces. *J. Fluid Mech.* **630**, 179.

Derksen, J.J. & Akker, H.E.A. Van Den 2007 Multi-scale simulations of stirred liquid-liquid dispersions. *CHem. Eng. Res.* **85**, 697.

Hinze, J.O. 1955 Fundamentals of the hydrodynamic mechanism of splitting in dispersion processes. *A.I.Ch.E. Journal* **1**, 289.

Kareem, W.A., Izawa, S., Xiong, A-K & Fukunishi, Y. 2009 Lattice boltzmann simulations of homogeneous isotropic turbulence. *Comp. Math. Appl.* **58**, 1055.

Qian, D., McLaughlin, J.B., Sankaranarayanan, K., Sundaresan, S. & Kontomaris, K. 2006 Simulation of bubble breakup dynamics in homogeneous turbulence. *Chem. Eng. Comm.* **193**, 1038.

Sbragaglia, M., Benzi, R., Biferale, L., Succi, S., Sugiyama, K. & Toschi, F. 2007 Generalized lattice boltzmann method with multirange pseudopotential. *Phys. Rev. E* **75** (2), 026702.

Shan, X. & Chen, H. 1993 Lattice boltzmann model for simulating flows with multiple phases and components. *Phys. Rev. E* **47**, 1815.

Shan, X. & Chen, H. 1994 Simulation of nonideal gases and liquid-gas phase transitions by the lattice boltzmann equation. *Phys. Rev. E* **49**, 2941.

Shan, X. & Doolen, G. 1995 Multicomponent lattice-boltzmann model with interparticle interaction. *J. Stat. Phys.* **81**, 379.

Succi, S. 2001 *The Lattice Boltzmann Equation for Fluid Dynamics and Beyond*. Oxford University Press, UK: Oxford.

Taylor, G.I. 1932 The viscosity of a fluid containing small drops of another fluid. *Proc. R. Soc. London, Ser. A* **138**, 41.

Taylor, G.I. 1934 The formation of emulsions in definable fields of flow. *Proc. R. Soc. London, Ser. A* **146**, 501.

Toschi, F. & Bodenschatz, E. 2009 Lagrangian properties of particles in turbulence. *Ann. Rev. Fluid Mech.* **41**, 375.

Voth, G.A., Crawford, A.M., Alexander, J. & Bodenschatz, E. 2002 Measurement of particle accelerations in fully developed turbulence. *J. Fluid Mech.* **469**, 121–160.

Voth, G.A., Satyanarayana, K. & Bodenschatz, E. 1998 Lagrangian accelaration measurements at large reynolds number. *Phys. Fluids.* **10**, 2268–2280.

Wolf-Galdrow, Dieter A. 2000 *Lattice gas cellular automata and lattice Boltzmann models: an introduction*. Springer Berlin Heidelberg New York: Springer.

Xi, H. & Duncan, C. 1998 Lattice boltzmann simulations of three-dimensional single droplet deformation and breakup under simple shear flow. *Phys. Rev. E* **59**, 3022.

Yu, H., Girimaji, S.S. & Luo, L-S. 2005 Lattice boltzmann simulations of decaying homogeneous isotropic turbulence. *Phys. Rev. E* **71**, 016708.